© 2017. Published by The Company of Biologists Ltd | Journal of Cell Science (2017) 130, 190-202 doi:10.1242/jcs.186031

SPECIAL ISSUE: 3D CELL BIOLOGY

RESEARCH ARTICLE

Increased ROS production in non-polarized mammary epithelial cells induces monocyte infiltration in 3D culture

Linzhang Li[1,2], Jie Chen[2], Gaofeng Xiong[2], Daret K. St Clair[3], Wei Xu[1,*] and Ren Xu[2,4,*]

ABSTRACT

Loss of epithelial cell polarity promotes cell invasion and cancer dissemination. Therefore, identification of factors that disrupt polarized acinar formation is crucial. Reactive oxygen species (ROS) drive cancer progression and promote inflammation. Here, we show that the non-polarized breast cancer cell line T4-2 generates significantly higher ROS levels than polarized S1 and T4R cells in three-dimensional (3D) culture, accompanied by induction of the nuclear factor κB (NF-κB) pathway and cytokine expression. Minimizing ROS in T4-2 cells with antioxidants reestablished basal polarity and inhibited cell proliferation. Introducing constitutively activated RAC1 disrupted cell polarity and increased ROS levels, indicating that RAC1 is a crucial regulator that links cell polarity and ROS generation. We also linked monocyte infiltration with disruption of polarized acinar structure using a 3D co-culture system. Gain- and loss-of-function experiments demonstrated that increased ROS in non-polarized cells is necessary and sufficient to enhance monocyte recruitment. ROS also induced cytokine expression and NF-κB activity. These results suggest that increased ROS production in mammary epithelial cell leads to disruption of cell polarity and promotes monocyte infiltration.

KEY WORDS: 3D cell culture, Tissue polarity, Reactive oxygen species, Inflammation, Monocyte infiltration, Breast cancer

INTRODUCTION

Tumors have been described as wounds that do not heal (Dvorak, 1986) because the two share some common features, such as chronic inflammation and disruption of normal tissue structure. Loss of cell polarity, an early cellular event during breast cancer development, is accompanied by substantial changes in the tumor microenvironment (Beliveau et al., 2010; Nelson and Bissell, 2006). Infiltration and differentiation of macrophages, the most abundant immune-related stromal cells in the tumor microenvironment (Allavena et al., 2008), correlate with poor prognosis in breast cancer patients, and drive cancer development and progression by inducing chronic inflammation (DeNardo et al., 2011; Medrek et al., 2012; Zhang et al., 2013). However, the connection between disruption of tissue polarity and macrophage infiltration remains to be determined.

[1]Department of Laboratory Medicine, The First Hospital of Jilin University, Changchun, Jilin Province 130021, China. [2]Markey Cancer Center, University of Kentucky, Lexington, KY 40536, USA. [3]Toxicology and Cancer Biology, University of Kentucky, Lexington, KY 40536, USA. [4]Department of Pharmacology and Nutritional Sciences, University of Kentucky, Lexington, KY 40536, USA.

*Authors for correspondence (ren.xu2010@uky.edu; xu_w@jlu.edu.cn)

R.X., 0000-0002-3591-9522

Received 12 January 2016; Accepted 17 August 2016

Cellular polarity is a fundamental property of normal epithelial tissue (Gudjonsson et al., 2002; Martin-Belmonte and Perez-Moreno, 2012). It has been shown that polarized tissue structure is crucial for maintaining tissue integrity and tissue-specific function (Inman and Bissell, 2010; Liu et al., 2004; Xu et al., 2009; Zeitler et al., 2004). In addition, cell adhesion and tight-junctions in polarized cells spatially segregate ligands and their receptors in epithelial sheets so that the activation of cell surface receptors and cell proliferation can be tightly and properly controlled (Ewald et al., 2012; Xu et al., 2009, 2010). Disruption of epithelial cell polarity leads to loss of tissue organization, increased susceptibility to carcinogenesis and eventual formation of tumors (Bilder, 2004; Bissell and Bilder, 2003; Weaver et al., 2002). A number of polarity regulators, including scribble, discs-large, and lethal giant larvae (which each have a number of different isoforms in mammals) have been identified as tumor suppressors (Bissell and Bilder, 2003; St Johnston and Ahringer, 2010; Tepass, 2012), indicating that the malignant transformation is strongly linked with loss of polarized tissue architecture (Bunker et al., 2015; Lee and Vasioukhin, 2008). Using the 3D culture model with the S1 and T4-2 cells lines of a tumor progression series, we and others have shown that disruption of tissue polarity is associated with remodeling of the tumor microenvironment (Becker-Weimann et al., 2013; Xiong et al., 2012).

Reactive oxygen species (ROS) such as hydrogen peroxide, superoxide and the hydroxyl radical, are byproducts of normal metabolism through the electron transport chain (Chance et al., 1979), and phagocyte-derived oxidants serve a protective function with respect to oxidant injury under normal physiological conditions (Babior, 2000). However, ROS and associated oxidative stress are considered a driving force for cancer development and progression (Cairns et al., 2011; Kamp et al., 2011). ROS induce oxidative damages in DNA, lipids, proteins and other cellular components and the damage is sufficient to induce malignant transformation (Cooke et al., 2003; Valko et al., 2006). In addition, ROS act as secondary signaling intermediates that control cellular phenotype (Droge, 2002; Finkel, 2003; Miao and St Clair, 2009; Puri et al., 2002). For example, matrix metalloproteinase-3 (MMP-3)-induced ROS are both necessary and sufficient to induce the epithelial–mesenchymal transition phenotypic alterations in target mammary epithelial cells (Radisky et al., 2005).

Chronic inflammation is accompanied by increased production of tissue ROS, which in turn can promote the inflammatory response by inducing transcription factors such as nuclear factor κB (NF-κB) and activator protein 1 (AP-1) (Kroncke, 2003; Li and Karin, 1999; Reuter et al., 2010). Constitutive activation of NF-κB in cancer cells leads to a variety of pro-tumorigenic effects (Hoesel and Schmid, 2013; Karin, 2009). By contrast, the NF-κB pathway in immune cells is a central regulator of the immune responses and is required for tumor-immunosurveillance. Given

Journal of Cell Science

Journal of Cell Science (2017) 130, 190-202 doi:10.1242/jcs.186031

the dual and differing roles of NF-κB in cancer development, a more-complete understanding of NF-κB pathway activation in cancer cells is crucial in order to specifically target this pathway in cancer tissue.

Our findings demonstrate that loss of polarity in mammary acini is associated with increased ROS production. Reducing ROS levels reprograms the non-polarized T4-2 cells to form polarized spheroids in 3D culture, whereas increased ROS production in polarized S1 cells is sufficient to disrupt basal polarity. Using a 3D co-culture system, we also found that elevated ROS levels in non-polarized cells induced monocyte infiltration, NF-κB activation and cytokine expression. These results established a potential link between tissue polarity, ROS generation and inflammation.

RESULTS

Disruption of the polarized acinar structure is associated with increased ROS production

ROS promote cancer initiation and progression (Moller and Wallin, 1998), but the function of ROS in regulating tissue polarity has not been determined. We first asked whether disruption of the polarized acinar structure is associated with increased ROS production. The 3D culture system of the human breast cancer progression series HMT-3522 (the non-malignant S1 cell line and its malignant counterpart T4-2) is a physiologically relevant model to investigate epithelial cell polarity and cancer progression (Kenny et al., 2007; Lelievre et al., 1998; Petersen et al., 1992; Weaver et al., 1997). The non-malignant S1 cells, in response to cues from 3D laminin-rich basement membrane (lrBM), form phenotypically normal, polarized and growth-arrested structures similar to those found *in vivo* in the terminal ductal lobular units of the breast (Fig. 1A). In contrast, the tumorigenic T4-2 cells accumulate additional and numerous genomic alterations during transformation, and these cells form large non-polarized structures. Treatment with the epidermal growth factor receptor inhibitor tyrphostin AG 1478 (TYR), MMP inhibitor GM6001, or phosphoinositide 3-kinase (PI3K) inhibitor LY294002 reprograms T4-2 cells to reestablish basal polarity (T4R) (Fig. 1A). To evaluate ROS levels, non-polarized T4-2 and polarized S1 and T4R cells in 3D Matrigel were stained with CellROX Deep Red, followed by live-cell imaging and quantification. We found higher levels of ROS in the non-polarized T4-2 cells compared to polarized S1 and T4R cells (Fig. 1B,C). These results suggest that disruption of the polarized acinar structure is associated with increased ROS production.

Disruption of acinar structure during cancer development is accompanied by loss of tissue polarity and increased cell proliferation. It has been shown that Akt1, an isoform of Akt, and RAC1 are key regulators of cellular proliferation and tissue polarity in the non-polarized mammary epithelial cells, respectively (Liu et al., 2004). We confirmed that introduction of RAC1 L61 (which has a Q61L mutation and is constitutively active) into T4-2 cells inhibited the restoration of polarity in response to TYR (Fig. 2A–C), but had little effect on cell proliferation (Fig. 2D,E). Importantly, we found that expression of RAC1 L61 significantly elevated ROS levels in TYR-treated T4-2 cells (Fig. 2F,G). Similar results were obtained in S1 cells (Fig. 2H,I; Fig. S1) and MCF-10A cells (Fig. 2J,K; Fig. S2). However, expression of the dominant-active Akt1 (Myr-Akt) only slightly increased ROS levels in TYR-treated T4-2 cells, although cell proliferation was significantly increased (Fig. 2D–G). These results suggest that increased ROS levels are associated with disruption of cell polarity and that RAC1 is a major regulator of ROS production in non-polarized mammary epithelial cells.

Elevation of ROS is necessary and sufficient to disrupt polarized acinar formation

To investigate whether increased ROS levels contribute to the disruption of polarized acinar structures in 3D culture, we lowered ROS in T4-2 cells using antioxidant N-acetyl-L-cysteine (NAC) or the reduced form of L-glutathione (GSH). NAC and GSH neutralize intracellular and extracellular ROS, providing a means to investigate the role of ROS in biological processes. T4-2 cells were cultured in Matrigel with NAC (4 mM) or GSH (4 mM) for 4 days to allow spheroid formation. The treatment significantly reduced intracellular levels of ROS (Fig. 3A,B). Immunofluorescence and confocal analysis showed that T4-2 cells formed polarized spheroids in the presence of NAC or GSH (Fig. 3C,D). The size of the T4-2 colony was significantly reduced in the NAC- or GSH-treated cells. Ki-67 staining showed that scavenging ROS attenuated T4-2 cell proliferation (Fig. 3E,F).

Glucose oxidase is an oxi-reductase, catalyzing the conversion of glucose into glucolactone, which is further converted into glucuronic acid and H_2O_2. It has been shown that treatment with glucose oxidase increases ROS levels in high-glucose medium (Kumar and Sitasawad, 2009; Wang et al., 2012). To determine whether increased ROS levels are sufficient to disrupt tissue polarity in 3D culture, we treated S1 cells with glucose oxidase. Treatment increased ROS levels (Fig. 4A,B), disrupted basal polarity (Fig. 4C,D), and induced cell proliferation in S1 cells (Fig. 4E,F). The same treatment also disrupted basal polarity in MCF10A cells (Fig. 4G–J) and TYR-treated T4-2 cells (Fig. S3). Importantly, reducing ROS levels with NAC (Fig. 4A,B) rescued cell polarization and inhibited cell proliferation in the glucose-oxidase-treated S1 cells (Fig. 4C–F). Collectively, these results indicate that increased ROS production is sufficient to impair polarized acinar morphogenesis.

Disruption of polarized acinar structure promotes monocyte infiltration by elevating ROS levels

Monocytes in peripheral circulation are recruited to tumor sites by chemotactic cytokines from tumor tissue, and are then differentiated to tumor-associated macrophages (Murdoch et al., 2004). Macrophage infiltration and differentiation has also been detected in ductal carcinoma *in situ* (Sharma et al., 2010; Wang et al., 1989). Macrophages also accumulate around the terminal end buds of mammary glands rather than near polarized ductal epithelial cells (Gouon-Evans et al., 2000; Ingman et al., 2006). One common feature shared by the terminal end buds and mammary tumor tissue is the presence of multilayered non-polarized epithelial cells. Therefore, we asked whether non-polarized mammary epithelial cells induce recruitment of monocytes. To recapitulate the interaction of mammary epithelial cells with monocytes during breast tumorigenesis, we developed a 3D co-culture assay (Fig. 5A). S1, T4-2, and T4R cells were cultured in 3D Matrigel for 72 h, followed by addition of THP-1 cells into the culture medium and incubation for an additional 24–48 h. A substantial number of THP-1 (GFP-expressing) cells invaded into the Matrigel and adhered to the T4-2 colonies, but very few THP-1 cells adhered to S1 or T4R cells (Fig. 5B,C). THP-1 cells are derived from a patient with acute monocytic leukemia, and this cell line has been used to study the function and differentiation of monocytes (Auwerx, 1991; Tsuchiya et al., 1982, 1980). To confirm our finding using primary human monocytes, CD14-positive monocytes (Lonza) were labeled with Cell Tracker Green (CMFDA) and co-cultured with S1, T4-2 and

Journal of Cell Science (2017) 130, 190-202 doi:10.1242/jcs.186031

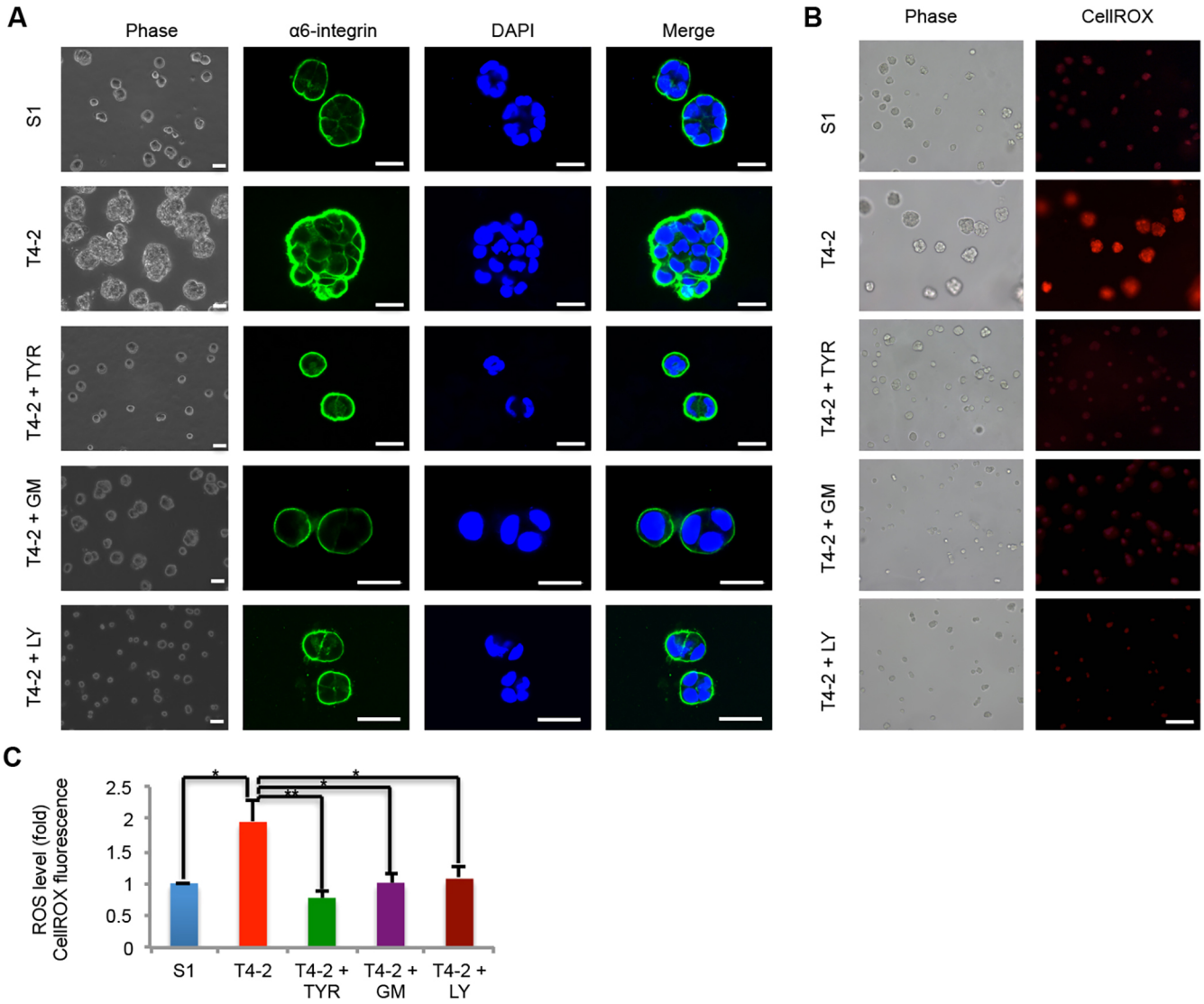

Fig. 1. Disruption of the polarized acinar structure is associated with increased ROS production. (A) Representative phase-contrast and immunofluorescence microscopy images of S1, T4-2 and phenotypically reversed T4-2 (T4R) cells in 3D culture. T4-2 cells were phenotypically reversed by tyrphostin AG 1478 (TYR), an EGFR inhibitor; GM6001 (GM), a MMP inhibitor; or LY294002 (LY), a PI3K inhibitor. Cell polarity was authenticated using the basal marker α6-integrin. S1 and T4R cells formed polarized spheroids, but T4-2 cells formed disorganized structures. Blue, DAPI; green, α6-integrin. Scale bars: 20 µm. (B) Cellular ROS levels were assessed in live S1, T4-2 and T4R cells by CellROX Deep Red reagent. S1, T4-2 and T4R cells were 3D cultured for 4 days, then incubated in the presence of CellROX Deep Red. Left panel, bright-field image; right panel, fluorescence image. Scale bar: 100 µm. (C) Quantitative imaging analysis of ROS detected by CellROX Deep Red in live S1, T4-2 and T4R cells. The images of individual ROS are presented in grayscale for assessment of the fluorescence intensity. Fluorescence intensity was assessed using Nikon NIS-Elements AR software. Experiments are in triplicate and presented data are the mean±s.e.m. *P<0.05, **P<0.01 (one-way ANOVA).

T4R cells as outlined above. As with the monocyte cell line, we found that these primary monocytes were recruited to the T4-2 colonies after 12 h of co-culture, whereas few monocytes migrated to S1 or T4R cells (Fig. 5D,E).

To decouple the effect of cell polarity and cell proliferation on monocyte infiltration, we performed co-culture experiments using RAC1 L61- and Myr-Akt-expressing T4-2 cells. We found that RAC1 L61 but not Myr-Akt rescued monocyte infiltration in TYR-treated T4-2 cells (Fig. 5F,G). These results suggest that monocyte infiltration is associated with disruption of polarity of mammary epithelial cells.

Next, we asked whether reducing ROS levels in T4-2 cells suppressed monocyte recruitment in the 3D co-culture assay. We found that treatment with NAC or GSH in T4-2 cells blocked THP-1 (Fig. 6A,B) and primary monocyte recruitment (Fig. 6C,D). We showed that treatment with glucose oxidase elevated ROS levels in S1 cells. To determine whether increased ROS generation is sufficient to induce THP-1 infiltration, we performed 3D co-culture with control and glucose-oxidase-treated S1 cells. We found that increased ROS generation, induced by glucose oxidase, significantly enhanced THP-1 recruitment (Fig. 6E,F). More interestingly, NAC prevented THP-1 infiltration induced by glucose oxidase (Fig. 6E,F). These results suggest that increased ROS production in non-polarized mammary epithelial cells induces monocyte infiltration during cancer progression.

ROS enhance cytokine expression and NF-κB activity in the non-polarized mammary epithelial cells

Monocyte infiltration and differentiation is largely regulated by cytokines (Coussens and Werb, 2002; Nathan, 2002). To determine

Journal of Cell Science (2017) 130, 190-202 doi:10.1242/jcs.186031

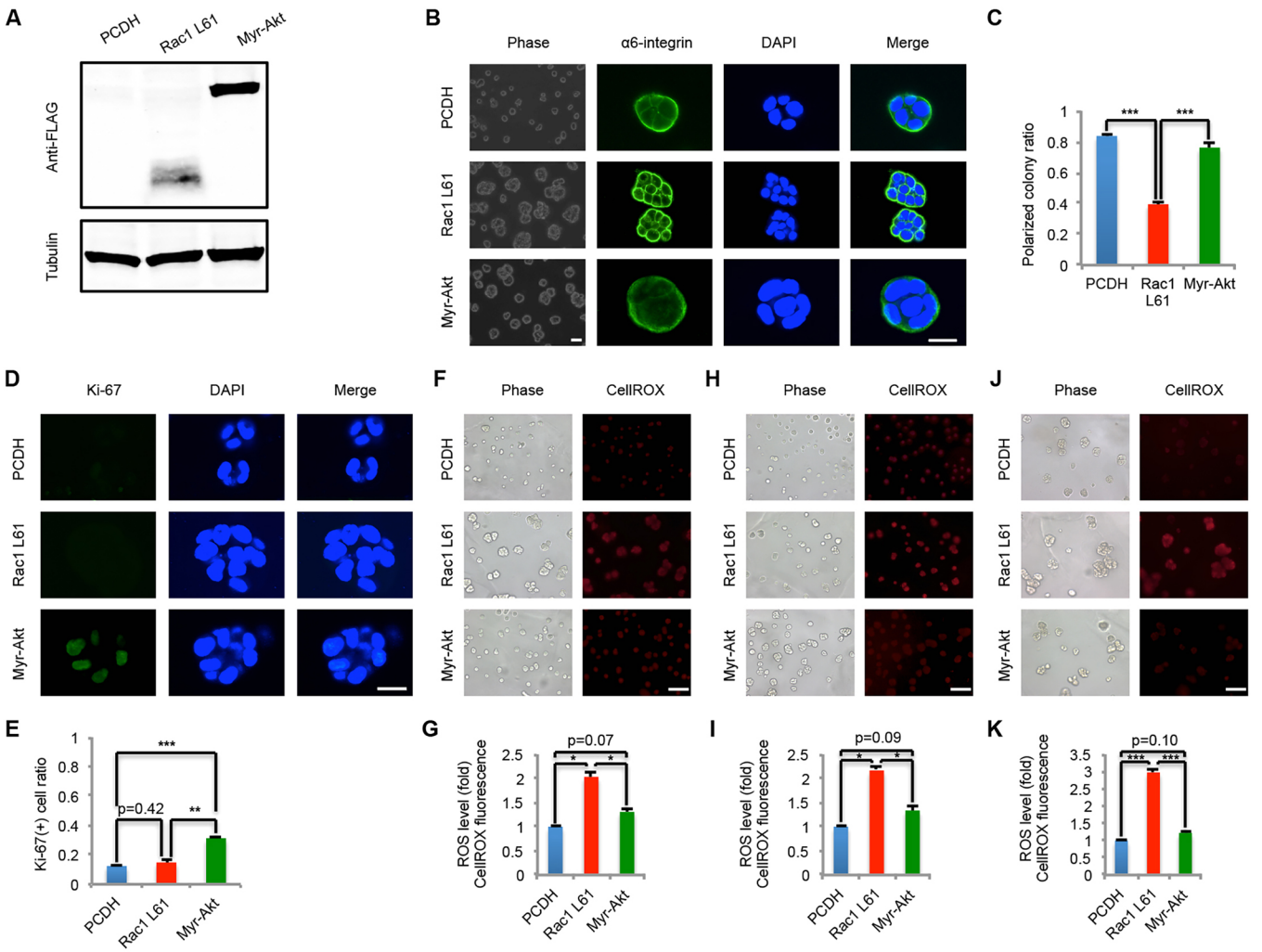

Fig. 2. Activation of RAC1 impairs polarization and increases ROS levels in mammary epithelial cells. T4-2 cells were infected with lentivirus containing either the RAC1 L61 or Myr-Akt expression constructs (PCDH, empty pCDH-CMV-MCS-EF1-Puro expression vector). (A) Western blot analysis demonstrating expression of constitutively active RAC1 L61 and Myr-Akt in T4-2 cells. (B) Expression of constitutively active RAC1 L61, but not Myr-Akt, rescued non-polarized tissue structures in TYR-treated T4-2 cells. Phase (left panel) and confocal (right-hand three panels) images show the morphology and α6-integrin staining of RAC1 L61- and Myr-Akt-expressing T4-2 cells. Blue, DAPI; green, α6-integrin. Scale bars: 20 µm. (C) Bar graph showing the ratio of polarized to total colonies in 3D culture from experiments as outlined in B. Experiments are in triplicate, and presented data are the mean±s.e.m. (n=3 each). ***P<0.001 (one-way ANOVA). (D) Proliferation in T4-2 cells treated as outlined in B was investigated by staining for Ki-67. Blue, DAPI; green, Ki-67. Scale bar: 20 µm. (E) Graphical representation that the ratio of Ki-67-positive to total cells was significantly increased in Akt-activated T4-2 cells in the presence of TYR. Presented data are the mean±s.e.m. (n=3). **P<0.01; ***P<0.001 (one-way ANOVA). (F) CellROX staining analysis of ROS level in RAC1 L61- and Myr-Akt-expressing T4-2 cells in the presence of TYR. Representative images are bright field (left panel) and fluorescence (right panel). Scale bar: 100 µm. (G) Graphical representation of ROS level in TYR-treated T4-2 cells treated with CellROX as outlined in F. Presented data are the mean±s.e.m. of triplicate experiments. *P<0.05 (one-way ANOVA). Staining (H) and graphical representation (I) of ROS levels in RAC1 L61- and Myr-Akt-expressing S1 cells determined by using the CellROX Deep Red method outlined above. Representative images are bright field (left panel), and fluorescence (right panel). Scale bar: 100 µm. Presented data are the mean±s.e.m. of triplicate experiments, with n=3 each. *P<0.05 (one-way ANOVA). Staining (J) and graphical representation (K) of ROS levels in RAC1 L61- and Myr-Akt-expressing MCF-10A cells determined by using the CellROX Deep Red dye. Representative images are bright field (left panel), and fluorescence (right panel). Scale bar: 100 µm. Presented data are the mean±s.e.m. of triplicate experiments, with n=3 each. ***P<0.001 (one-way ANOVA).

whether loss of tissue polarity enhances cytokine expression and subsequently promotes monocyte infiltration, we compared expression of cytokine genes in non-polarized T4-2 cells with expression in polarized S1 and T4R cells. Quantitative real-time (q) RT-PCR demonstrated that the cytokines interleukin (IL)-24, CXCL1, CXCL3 and CXCL8 were significantly upregulated in non-polarized T4-2 cells compared to polarized S1 and T4R cells (Fig. 7A). Although expression of IL-6 and IL-32 was upregulated in T4-2 cells compared to S1 cells, mRNA levels of IL-6 and IL-32 were not significantly altered in T4R cells compared to T4-2 cells (Fig. 7A). We also found that disruption of tissue polarity with constitutively activated RAC1 in TYR-treated T4-2 cells significantly enhanced the cytokine mRNA expression, whereas dominant-activated Akt only slightly increased the expression (Fig. 7B). To examine whether the secretion of cytokines is increased in non-polarized cells, we evaluated protein levels of IL-6 and CXCL-1 by examining conditioned medium collected from S1 and T4-2 cells with enzyme-linked immunosorbent assay (ELISA). We found that secretion of IL-6 and CXCL-1 was significantly increased in the T4-2 cells compared to the S1 cells (Fig. 7C).

We have recently shown that NF-κB is activated in the non-polarized T4-2 cells (Becker-Weimann et al., 2013). We measured

Journal of Cell Science (2017) 130, 190-202 doi:10.1242/jcs.186031

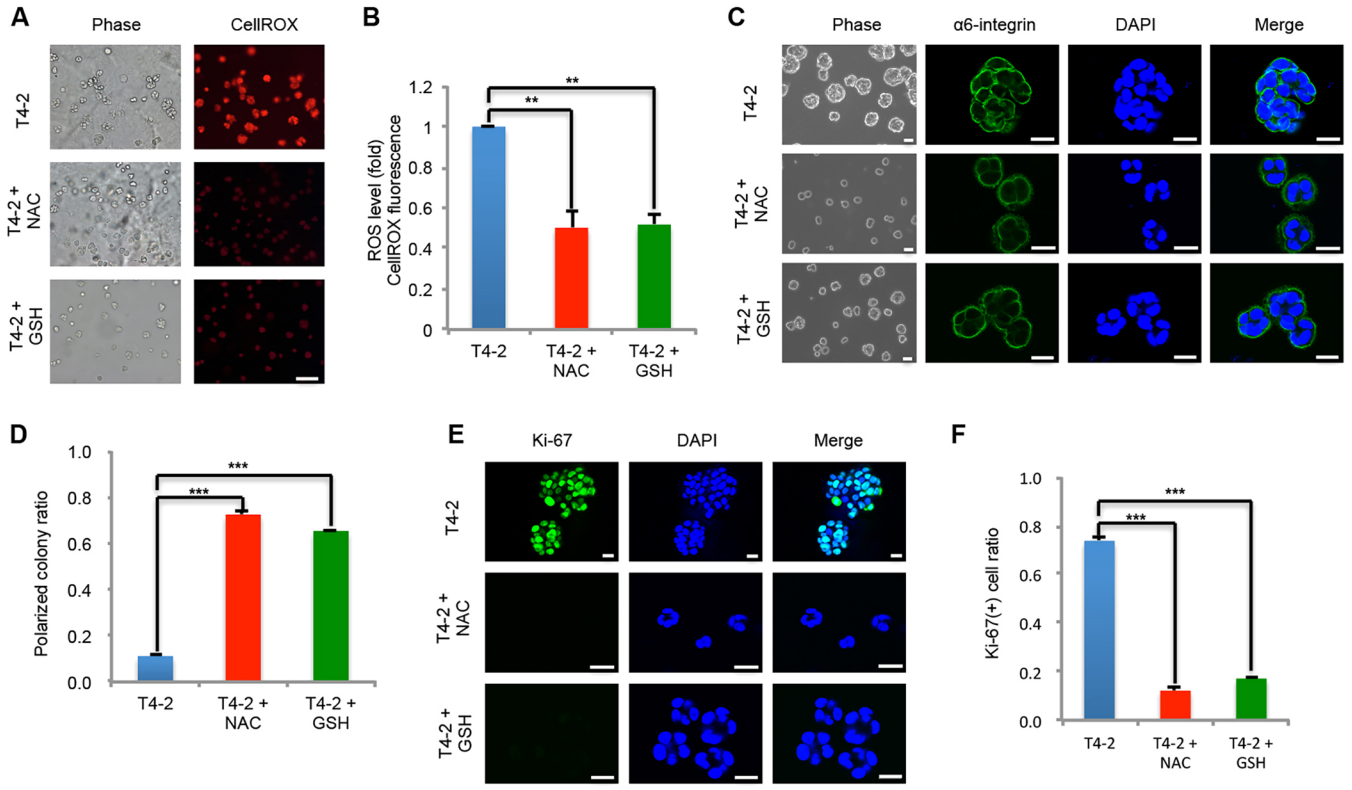

Fig. 3. Suppression of ROS levels reprograms T4-2 cells to form polarized acini. (A) Antioxidant N-acetyl-L-cysteine (NAC) or reduced L-glutathione (GSH) reduces ROS levels in 3D cultured T4-2 cells. T4-2 cells were cultured in the presence or absence of 4 mM NAC or GSH for 4 days in Matrigel, and then stained with CellROX. Representative images are bright field (left panel) and fluorescence (right panel). Scale bar: 100 µm. (B) Graphical representation of the fluorescence intensity in T4-2 and T4-2 treated with NAC or GSH as outlined above. Presented data are the mean±s.e.m. of triplicate experiments. $^{**}P<0.01$ (one-way ANOVA). (C) T4-2 cells were cultured in Matrigel for 4 days in the presence or absence of 4 mM NAC or GSH, and basal polarity was assessed by α6-integrin staining. Representative images are bright field (left panel) and fluorescence (three right panels). Blue, DAPI; green, α6-integrin. Scale bars: 20 µm. (D) Graphical representation of polarized colonies presented as a ratio of polarized to total colonies. Presented data are the mean±s.e.m. of triplicate experiments. $^{***}P<0.001$ (one-way ANOVA). (E) Cell proliferation and apoptosis were assessed by Ki-67 immunostaining. Blue, DAPI; green, Ki-67. Scale bars: 20 µm. (F) Graphical representation of the ratio of Ki-67-positive to total cells in control and NAC- or GSH-treated T4-2 cells. Presented data are the mean±s.e.m. of triplicate experiments. $^{***}P<0.001$ (one-way ANOVA).

luciferase activity in T4-2 cells stably transfected with the 3X-κB-L reporter plasmid, and results showed that NF-κB activity was significantly reduced in T4R cells (Fig. 7D). Nuclear levels of the NF-κB p65 subunit (also known as RELA) also decreased in T4R cells compared to control T4-2 cells (Fig. 7E). NF-κB is a redox-sensitive transcription factor regulating cytokine expression and inflammation (Baldwin, 1996; Morgan and Liu, 2011). We found that treatment with the NF-κB inhibitor Wedelolactone in T4-2 cells significantly reduced mRNA levels of cytokines (Fig. 7F). We also showed that RAC1 L61 but not Myr-Akt induced the NF-κB-driven luciferase activity in TYR-treated T4-2 cells (Fig. 7G). These results suggest that activation of the NF-κB cascade in non-polarized T4-2 cells at least partially mediates induction of inflammation-related cytokine expression.

To determine whether induction of cytokine expression is regulated by ROS in non-polarized mammary epithelial cells, we assessed the cytokine expression in control and NAC-treated T4-2 cells. We found that NAC treatment significantly inhibited mRNA expression of IL-6, IL-24, CXCL1, CXCL2, CXCL3 and CXCL8 in T4-2 cells (Fig. 8A). In addition, secretion of IL-6 and CXCL1 into the culture medium was significantly reduced in NAC-treated T4-2 cells (Fig. 8B). To determine whether ROS are sufficient to induce cytokine expression in mammary epithelial cells, ROS production was induced in S1 cells through glucose oxidase treatment. Increased ROS production significantly enhanced expression of cytokine genes (Fig. 8C), and Wedelolactone treatment repressed the cytokine expression induced by glucose oxidase (Fig. 8C). Next, we determined whether NAC or GSH treatment inhibits NF-κB activity in T4-2 cells. Luciferase reporter analysis data showed that the transactivation activities of NF-κB were significantly inhibited in T4-2 cells when ROS production was inhibited by NAC or GSH (Fig. 8D). Immunoblot analysis revealed that nuclear p65 protein levels were decreased in T4-2 cells when ROS were reduced by NAC (Fig. 8E). These results suggest that scavenging of ROS inhibits cytokine expression through downregulation of NF-κB activities.

DISCUSSION

Disruption of the polarized epithelial tissue structure occurs at the early stage of breast cancer development (Bissell et al., 2002; Boghaert et al., 2014; Debnath and Brugge, 2005; Muthuswamy and Xue, 2012) and is associated with substantial remodeling of the tissue microenvironment. Breast cancer is characterized by tumor-associated macrophage infiltration (DeNardo and Coussens, 2007; Leek et al., 1996; Mahmoud et al., 2012). Monocytes in the peripheral circulation are recruited to the tumor site by chemotactic cytokines from tumor tissue, and are then differentiated to tumor-associated macrophages (Murdoch et al., 2004). Macrophage

Journal of Cell Science (2017) 130, 190-202 doi:10.1242/jcs.186031

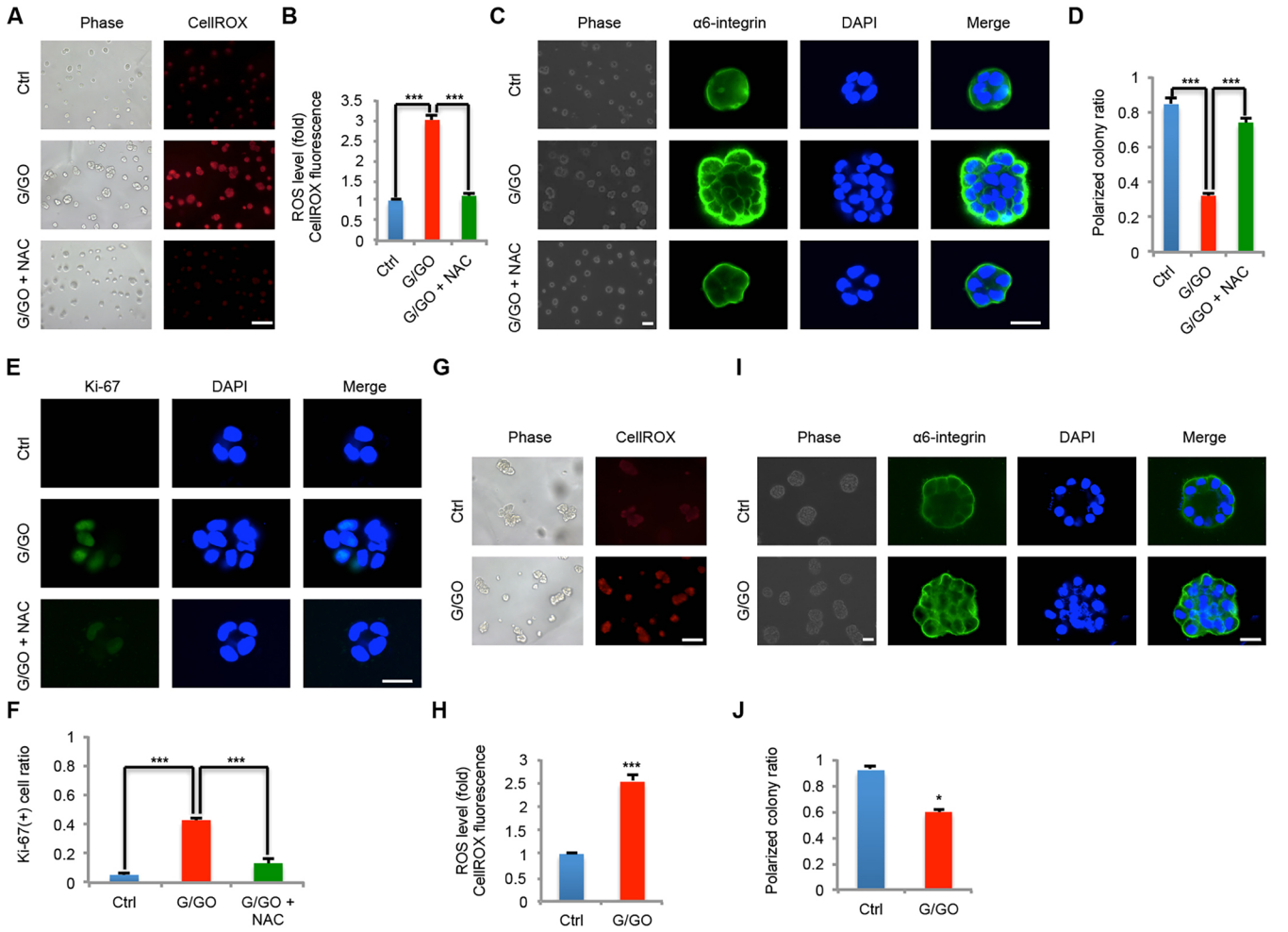

Fig. 4. Increase in ROS levels disrupts basal polarity in S1 and MCF-10A cells. (A) ROS were detected in S1 cells treated with 20 mM glucose and 1.0 mU glucose oxidase (denoted G/GO) using the CellROX method. S1 cells were treated with G/GO in the absence or presence of NAC (4 mM) in Matrigel for 6 days. Representative images are bright field (left panel) and fluorescence (right panel). Scale bar: 100 µm. (B) Graphical representation of ROS levels in control, G/GO-treated, and G/GO plus NAC-treated S1 cells. Presented data are mean±s.e.m. with n=3 each. ***P<0.001 (one-way ANOVA). (C) Representative images of phase (left) and confocal (three right-hand panels) α6-integrin staining showing basal polarity in control, G/GO-treated and G/GO- plus NAC-treated S1 cells. Blue, DAPI; green, α6-integrin. Scale bars: 20 µm. (D) Graphical representation of data from cells in C shows that G/GO treatment significantly reduced the number of polarized S1 colonies in 3D culture. Treatment with NAC partially rescued polarization in G/GO-treated cells. Presented data are the mean±s.e.m. with n=3 each. ***P<0.001 (one-way ANOVA). (E) Representative image of Ki-67 staining showing that G/GO treatment slightly increased proliferation in S1 cells. Blue, DAPI; green, Ki-67. Scale bar: 20 µm. (F) Graphical representation of the ratio of Ki-67-positive to total cells treated with G/GO in the absence or presence of NAC. Presented data are the mean±s.e.m. with n=3 each. ***P<0.001 (one-way ANOVA). (G) ROS levels were detected on day 8 by the CellROX method in control and G/GO-treated MCF-10A cells cultured in 3D. Representative images are bright field (left panel) and fluorescence (right panel). Scale bar: 100 µm. (H) Graphical representation of ROS levels in control and G/GO-treated MCF-10A cells. Presented data are the mean±s.e.m. with n=3. ***P<0.001 (Student's t-test). (I) Basal polarity was examined in control and G/GO-treated MCF-10A cells by α6-integrin staining. Representative images are bright field (left panel) and fluorescence (three right-hand panels). Scale bars: 20 µm. (J) Graphical representation of data obtained in I showing that G/GO treatment significantly reduced the number of polarized colonies in MCF-10A cells. Presented data are the mean±s.e.m. with n=3 each. *P<0.05 (Student's t-test).

accumulation has been detected in ductal carcinoma *in situ* (Sharma et al., 2010; Wang et al., 1989). Interestingly, macrophages also accumulate around the terminal end buds of mammary glands rather than near the polarized ductal epithelial cells (Gouon-Evans et al., 2000; Ingman et al., 2006). Mammary epithelial cells in the terminal end bud are multilayer and non-polarized (Ewald et al., 2012; Rejon and McCaffrey, 2015). These results suggest that macrophage infiltration is associated with loss of tissue polarity. Using the 3D culture model of mammary tumor progression, we demonstrate that loss of tissue polarity is associated with ROS generation, increased cytokine expression and monocyte infiltration (Fig. 5C), providing new insight into the regulation of cancer-associated inflammation.

Deregulated ROS generation contributes to development of cancer and inflammation (Colotta et al., 2009; Hanahan and Weinberg, 2011), but its function and regulation in the disruption of tissue polarity has not been determined. Here, we demonstrate that ROS levels are significantly upregulated in non-polarized breast cancer cells compared to in polarized non-malignant cells (Fig. 1). Activation of RAC1 leads to the disruption of cell polarity in mammary epithelial cells. We show that introduction of a constitutively activated RAC1 is sufficient to induce ROS generation in mammary epithelial cells. It has been shown that activated RAC1 binds to and forms a complex with NOX1. NOX1 is a homolog of the phagocyte NADPH-oxidase component gp91^{phox} (also known as CYBB). NOX1 has the capacity to transport

Journal of Cell Science (2017) 130, 190-202 doi:10.1242/jcs.186031

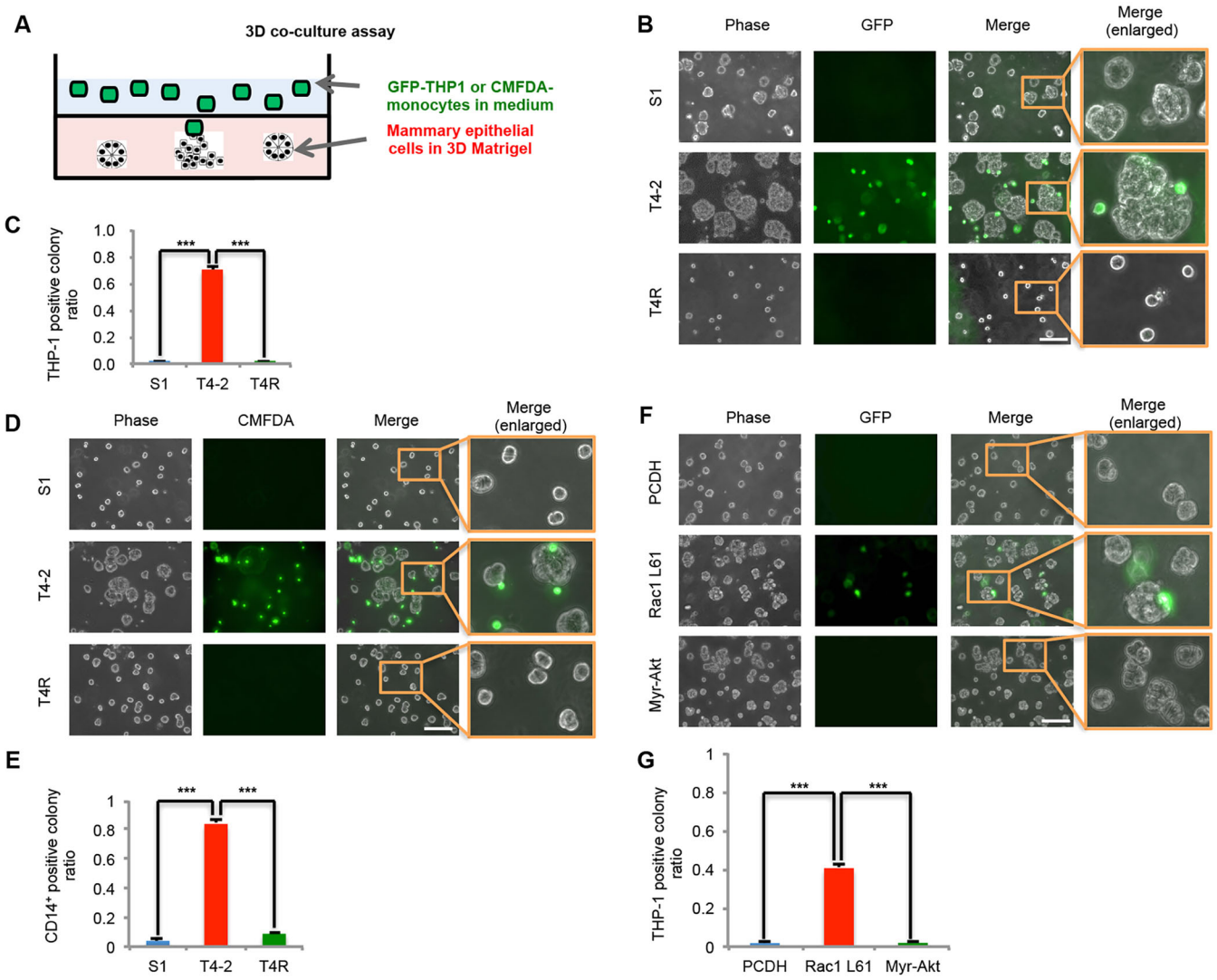

Fig. 5. Disruption of polarized acinar structure promotes monocyte infiltration. (A) Schematic of the complete 3D co-culture model. (B) Monocyte recruitment was assessed in the 3D co-cultured assay. Non-polarized T4-2 cells supported infiltration of THP-1 (GFP expressing) cells to a greater extent than did the polarized S1 and T4R cells. Representative images are bright field (left panel) and fluorescence (three right-hand panels). Scale bar: 100 µm. (C) Graphical representation of the ratio of THP-1-positive S1, T4-2 and T4R colonies in 3D co-culture. Presented data are the mean±s.e.m. with n=3 each. ***P<0.001 (one-way ANOVA). (D) 3D co-cultures of human CD14$^+$ monocytes (labeled with Cell Tracker Green CMFDA) and S1, T4-2 and T4R cells. Representative images are bright field (left panel) and fluorescence (three right-hand panels). Scale bar: 100 µm. (E) Graphical representation of data obtained in D. Presented data are the mean±s.e.m. (n=3). ***P<0.001 (one-way ANOVA). Polarized S1 and T4R cells significantly reduced the adherence of human CD14$^+$ monocytes. (F) 3D co-cultures of GFP-expressing THP-1 cells and TYR-treated T4-2 cells stably expressing constitutively active RAC1 L61 or Myr-Akt. Representative images are bright field (left panel) and fluorescence (three right-hand panels). PCDH, empty vector. Scale bar: 100 µm. (G) Constitutively activated RAC1 L61 but not Myr-Akt in TYR-treated T4-2 cells resulted in a significant increase in THP-1 infiltration using the 3D co-culture assay. Graphical representation of data obtained in F. Presented data are the mean±s.e.m. (n=3). ***P<0.001 (one-way ANOVA).

electrons across the plasma membrane and to generate superoxide and other downstream ROS. The binding of RAC1 induces activation of NOX1 and triggers the NOX1-dependent ROS generation (Cheng et al., 2006). These results indicate that RAC1 is a major regulator that integrates non-polarized tissue formation and ROS production.

ROS play crucial roles in cancer development and progression (Karin, 2006; Waris and Ahsan, 2006; Wiseman and Halliwell, 1996). We identified a new function of ROS in regulating the basal polarity of mammary epithelial cells. We show that increased ROS production is necessary and sufficient to disrupt the polarized acinar structure. ROS act as secondary signaling intermediates modulating multiple pathways (Droge, 2002; Finkel, 2011), and many of these pathways are involved in cell polarization. For instance, increased ROS production enhances the activity of FAK (also known as PTK2), an important regulator of cell polarity (Chiarugi et al., 2003; Vepa et al., 1999). In addition, H_2O_2 induces activation of both myosin light chain kinase (MLCK, also known as MYLK) and protein kinase C (PKC) in endothelial cells (Zhao and Davis, 1998). However, the downstream target of ROS that induces the disruption of polarized acinar structure in mammary epithelial cells is presently unknown.

Our findings demonstrate that ROS are important mediators of the cancer-cell–monocyte interaction in 3D co-culture. We show that ROS induce expression of multiple cytokine genes in non-polarized malignant cells. These cytokines might promote recruitment and

Journal of Cell Science (2017) 130, 190-202 doi:10.1242/jcs.186031

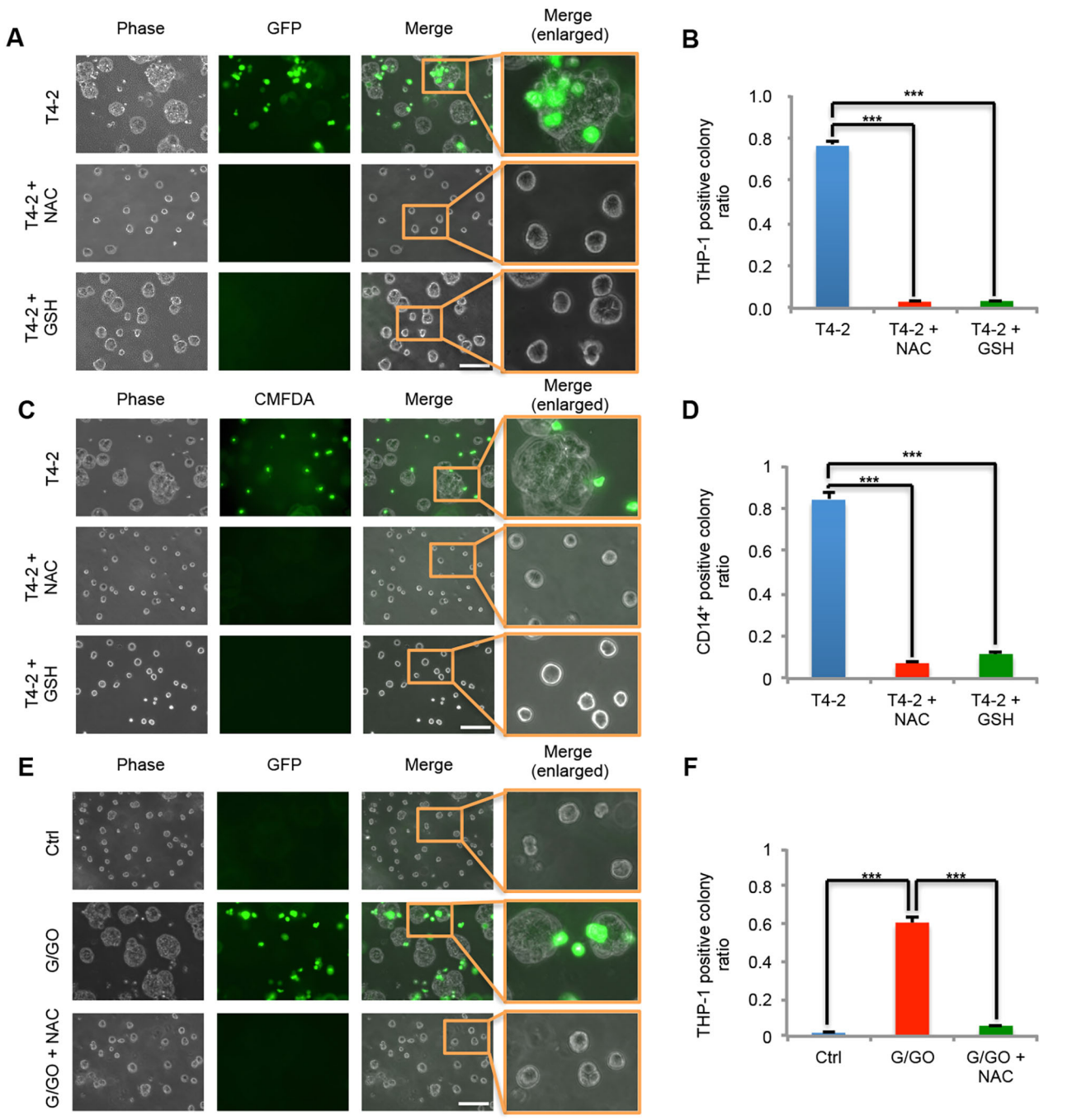

Fig. 6. Increased ROS production in non-polarized mammary epithelial cells induces monocyte recruitment. (A) Reducing ROS levels in T4-2 cells with antioxidants NAC or GSH inhibited the recruitment of THP-1 (GFP expressing) cells in the 3D co-culture assay. Representative images are bright field (left panel) and fluorescence (three right-hand panels). Scale bar: 100 µm. (B) Graphical representation of THP-1 recruitment in the 3D co-culture assay described in A. Presented data are the mean±s.e.m. (n=3). ***P<0.001 (one-way ANOVA). (C) Antioxidant NAC or GSH treatment in T4-2 cells significantly inhibited human CD14$^+$ monocyte (stained with Cell Tracker Green) infiltration in the 3D co-culture assay. Representative images are bright field (left panel) and fluorescence (three right-hand panels). Scale bar: 100 µm. (D) Graphical representation of primary monocyte recruitment in the 3D co-culture assay described in C. Presented data are the mean±s.e.m. (n=3). ***P<0.001 (one-way ANOVA). (E) Increased ROS levels in S1 cells with 20 mM glucose and 1.0 mU glucose oxidase (denoted G/GO) induced THP-1 recruitment in the 3D co-culture system, while NAC blocked THP-1 infiltration induced by G/GO. Representative images are bright field (left panel) and fluorescence (three right-hand panels). Scale bar: 100 µm. (F) Graphical representation of the ratio of THP-1-positive colonies in the 3D co-culture assay described in E. Presented data are the mean±s.e.m. (n=3). ***P<0.001 (one-way ANOVA).

infiltration of monocytes in 3D culture. We showed previously that disruption of polarized acinar structure induces the NF-κB pathway (Becker-Weimann et al., 2013). The constitutive activation of NF-κB impairs polarized acinar morphogenesis (Becker-Weimann et al., 2013). NF-κB is a redox-regulated sensor for oxidative stress and is activated by hydrogen peroxide (Bubici et al., 2006; Kim et al., 2014; Morgan and Liu, 2011). We found that reduction of ROS levels in T4-2 cells significantly inhibits NF-κB activity, indicating that the induction of NF-κB pathway in non-polarized mammary epithelial cells is ROS dependent. The primary regulation

Journal of Cell Science

Journal of Cell Science (2017) 130, 190-202 doi:10.1242/jcs.186031

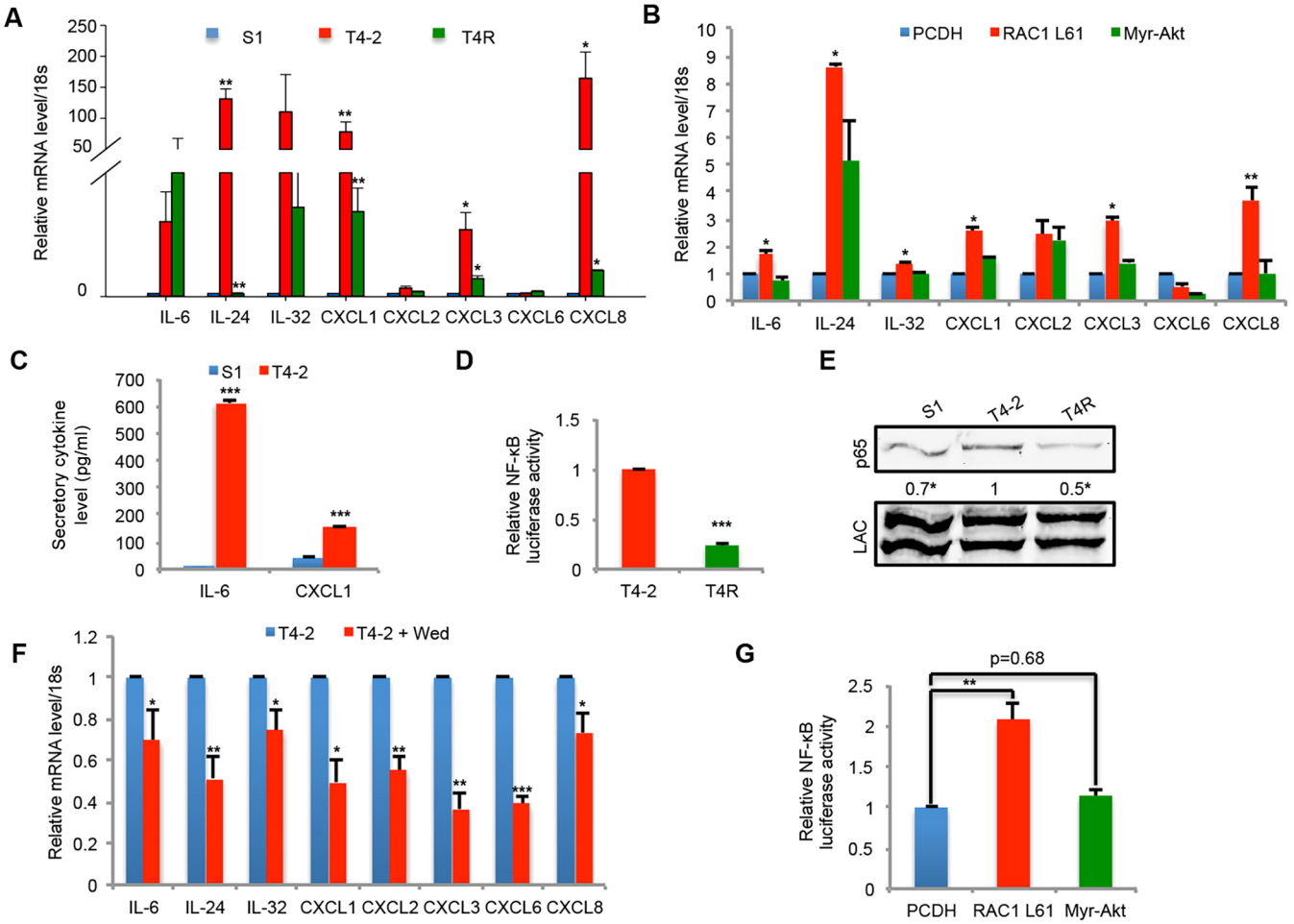

Fig. 7. NF-κB activation induces cytokine expression in the non-polarized mammary epithelial cells. (A) Expression of cytokines was upregulated in T4-2 cells compared to S1 and T4R cells. Graphical representation of qRT-PCR to detect cytokine expression in S1, T4-2 and T4R cells in 3D culture. Presented data are the mean±s.e.m. (n=3). *P<0.05, **P<0.01 (one-way ANOVA). (B) Graphical representation of cytokine expression as determined by qRT-PCR. Expression of RAC1 L61 in TYR-treated T4-2 cells significantly enhanced cytokine transcription, whereas expression of Myr-Akt only slightly increased the mRNA levels of cytokine genes. PCDH, empty vector. Presented data are the mean±s.e.m. (n=3). *P<0.05, **P<0.01 (one-way ANOVA). (C) Graphical representation of IL-6 and CXCL1 levels in conditioned medium collected from the same amount of S1 and T4-2 cells in 3D culture by ELISA. Presented data are the mean±s.e.m. of triplicate experiments. ***P<0.001 (Student's t-test). (D) Graphical representation of luciferase activity. Luciferase analysis of NF-κB transcription activities in T4-2 and T4R cells. Presented data are the mean±s.e.m. (n=3). ***P<0.001 (Student's t-test). (E) Western blot analysis of nuclear protein levels for p65 in S1, T4-2 and T4R cells. Fold activation levels were calculated by dividing the normalized values from S1 and T4R cells by that from T4-2 cells and are the mean of n=3. *P<0.05 (one-way ANOVA). (F) Graphical representation of cytokine expression determined by qRT-PCR. Treatment with NF-κB inhibitor Wedelolactone (Wed) significantly reduced cytokine expression in T4-2 cells. Presented data are the mean±s.e.m. (n=3). *P<0.05, **P<0.01, ***P<0.001 (Student's t-test). (G) Graphical representation of luciferase activity for NF-κB transcription in RAC1 L61 and Myr-Akt-expressing T4-2 cells in the presence of TYR. Presented data are the mean±s.e.m. (n=3). **P<0.01 (one-way ANOVA).

of the NF-κB pathway is through the association of NF-κB complexes with their inhibitor, IκB proteins; it binds to the p65 or p50 (encoded by *NFKB1*) subunit and inhibits nuclear translocation. ROS induce NF-κB activation through a modulation of DNA-binding activity or upstream NF-κB signaling pathways (Gloire et al., 2006; Morgan and Liu, 2011). It has been shown that ROS induce Src activation, and subsequently enhances PKD and IKKβ activation (Gloire et al., 2006; Morgan and Liu, 2011). The NF-κB pathway is a crucial regulator of cytokine expression and inflammation (Karin, 2009; Schreck et al., 1991). We also found that inhibition of the NF-κB pathway represses ROS-induced cytokine expression. These results suggest that ROS enhance cytokine expression and monocyte infiltration by inducing the NF-κB pathway in non-polarized breast cancer cells.

In summary, the finding that ROS contribute to the disruption of tissue polarity and monocyte infiltration significantly advances our understanding of cancer-associated inflammation. However, additional *in vivo* studies are needed to corroborate the importance of ROS in the regulation of tissue polarity as well as the central role of polarity in monocyte infiltration and inflammation.

MATERIALS AND METHODS

Reagents

Dulbecco's modified Eagle's medium (DMEM) with F12 and RPMI 1640 media were obtained from Sigma-Aldrich (St Louis, MO). Culture additives fetal bovine serum (FBS), transferrin, β-estradiol, and prolactin were obtained from Sigma; insulin was from Boehringer Mannheim (Indianapolis, IN), and sodium selenite, hydrocortisone and epidermal growth factor (EGF) were from BD Biosciences (Bedford, MA). N-acetyl-L-cysteine (NAC; A7250), reduced L-glutathione (GSH; G6013), Wedelolactone (Wede; W4016), G418 (A1720), D-(+)-glucose (G7021), glucose oxidase (G7141) were obtained from Sigma-Aldrich. DAPI was from Molecular Probes (D1306; Eugene, OR). Matrigel was obtained from BD Biosciences (354230; San Diego, CA).

Journal of Cell Science (2017) 130, 190-202 doi:10.1242/jcs.186031

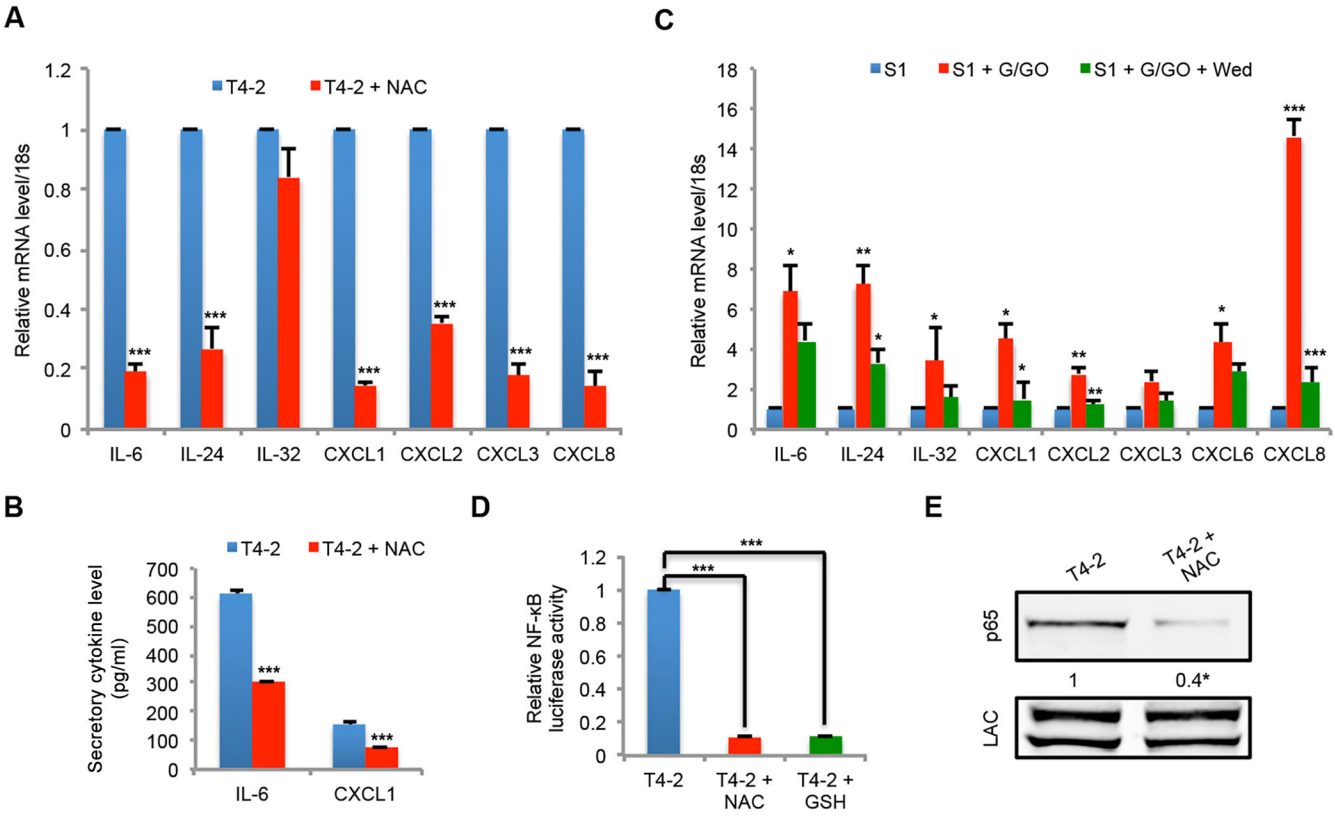

Fig. 8. Increased ROS production in non-polarized mammary epithelial cells significantly enhances cytokine expression and NF-κB activity. (A) Graphical representation of qRT-PCR analysis of cytokine expression in control and NAC-treated (4 mM) T4-2 cells. Treatment with NAC significantly inhibited cytokine expression in T4-2 cells. Presented data are the mean±s.e.m. (n=3). ***P<0.001 (Student's t-test). (B) Graphical representation of IL-6 and CXCL1 protein in conditioned medium collected from control and NAC-treated T4-2 cells as measured with ELISA. Presented data are the mean±s.e.m. (n=3). ***P<0.001 (Student's t-test). (C) Graphical representation of cytokine expression as determined by qRT-PCR. The NF-κB inhibitor Wedelolactone (Wed) prevented the induction in mRNA expression of some cytokines by 20 mM glucose and 1.0 mU glucose oxidase (G/GO) in 3D cultured S1 cells. Presented data are the mean±s.e.m. (n=3). *P<0.05, **P<0.01, ***P<0.001 (one-way ANOVA). (D) Graphical representation of luciferase activity for NF-κB-driven transcription in T4-2 cells in the presence or absence of NAC or GSH. Presented data are the mean±s.e.m. of triplicate experiments. ***P<0.001 (one-way ANOVA). (E) Western blot analysis of nuclear protein levels of p65 in control and T4-2 cells treated with NAC. Fold changes were determined by dividing the normalized values from NAC-treated cells by that of untreated T4-2 cells and are the mean for n=3. *P<0.05.

The antibodies used were obtained from the following companies: monoclonal rat anti-integrin α6 (555734, 1:500 dilution) from BD Biosciences; monoclonal rabbit anti-Ki-67 from Spring Bioscience (M3060; 1:250 dilution; Pleasanton, CA); Alexa-Fluor-488-conjugated goat anti-rat-IgG and Alexa-Fluor-488-conjugated goat anti-rabbit-IgG from Invitrogen (A11006, A11034; 1:500 dilution; Eugene, OR); polyclonal anti-p65 from Santa Cruz Biotechnology (sc-109; 1:1000 dilution; Santa Cruz, CA); monoclonal mouse anti-FLAG (F3165, 1:1000 dilution) from Sigma-Aldrich; polyclonal anti-lamin A/C (LAC; 1:1000 dilution; sc-20681) from Santa Cruz Biotechnology; monoclonal mouse anti-tubulin from Abcam (ab7291; 1:1000 dilution; Cambridge, MA); and Dylight-680-conjugated goat anti-rabbit-IgG from Thermo Scientific (35569; 1:1000 dilution; Rockford, IL).

Cell cultures in 2D and 3D

The HMT-3522 mammary epithelial cells (a kind gift from Mina Bissell, Lawrence Berkeley National Laboratory, Berkeley, CA) were cultured in T4 medium consisting of DMEM/F12 with 250 ng/ml insulin, 10 µg/ml transferrin, 2.6 ng/ml sodium selenite, 10^{-10} M β-estradiol, 1.4 µM hydrocortisone and 5 µg/ml prolactin. The non-neoplastic S1 cells were cultured in T4 medium with 10 ng/ml EGF. The malignant T4-2 cells were cultured on collagen type I pre-coated dishes in the absence of EGF. T4 medium was routinely changed every 2–3 days. Cells were grown in a humidified incubator at 37°C with 5% CO_2.

For the 3D laminin-rich extracellular matrix (3D lrECM) 'On-Top' assay, 250 µl of cell suspension in T4 medium was seeded on top of a thin gel of Engelbreth–Holm–Swarm (EHS) tumor extract (Matrigel; 125 µl) in a 24-well plate. S1 cells were seeded at a density of 5.0×10^4 cells/cm^2 and T4-2 cell lines were seeded at 4.0×10^4 cells/cm^2. This cell suspension, on top of Matrigel, was incubated at 37°C for 60 min. To reverse the malignant phenotypes of T4-2 (T4R) cells, 250 µl T4 medium containing 10% Matrigel with different inhibitors were added to the culture with a final concentration of 100 nM (Tyrphostin AG1478, Sigma), 10 µM (LY 294002, Sigma) or 50 µM (GM6001, Calbiochem). Media with the inhibitors were changed every 2 days in the next 4 days.

THP-1 cells (a kind gift from Philip A. Kern, University of Kentucky, Lexington, KY) were cultured in RPMI 1640 medium with 10% fetal bovine serum (FBS) and 1% penicillin-streptomycin (Sigma), supplemented with 2-mercaptoethanol (0.05 mM, MP Biomedicals). The PCDH–GFP construct (System Biosciences) was transfected into THP-1 cells, and then selected over 2 weeks with puromycin until more than 90% of the cells were GFP positive.

MCF-10A cells (a kind gift from Michael W. Kilgore, University of Kentucky, Lexington, KY) were cultured in 2D or 3D as previously described (Debnath et al., 2003).

3D co-culture assay

The cells were cultured in 3D Matrigel for 3 days using the 'On Top' protocol in a 24-well plate as described above. To remove TYR, NAC, GSH or glucose oxidase in 3D culture, the medium was replaced with T4 medium (chemical free) and washed twice before seeding THP-1 (GFP expressing) cells (40,000 cells/well). Bright-field and fluorescence images were taken 24–48 h later with an Eclipse Ti workstation (Nikon). The pictures were taken under fixed exposure conditions.

Human peripheral blood $CD14^+$ monocyte cells (Lonza, 2W-400C) were labeled with Cell Tracker Green CMFDA (Molecular Probes, C2925) according to the manufacturer's instructions. Briefly, $CD14^+$ monocyte cells were harvested by centrifugation and resuspended in a 15-ml tube with 3 ml pre-warmed serum-free RPMI 1640 medium containing 10 µM CMFDA. The labeled $CD14^+$ monocyte cells were placed on top of mammary epithelial cells in 3D culture (24-well plate, 40,000 cells/well). Bright-field and fluorescence images were taken 12 h later with an Eclipse Ti workstation (Nikon).

DNA constructs and gene transfection

FLAG-tagged RAC1 L61 and FLAG-tagged Myr-Akt Δ4-129 were amplified from constructs pcDNA3-EGFP-RAC1-Q61L (Addgene plasmid # 12981) and myrAkt delta4-129 (Addgene plasmid # 10841) respectively, and cloned into the pCDH-CMV-MCS-EF1-Puro (PCDH) expression vectors (System Biosciences). 293 FT cells were transfected with PCDH, PCDH-RAC1 L61 or PCDH-Myr-Akt, plus packaging lentivector using the FuGENE HD Transfection Reagent to produce lentivirus stocks. HMT-3522 mammary epithelial cells or MCF-10A cells were infected with lentivirus and selected by puromycin after 48 h of infection.

ROS staining and detection

ROS measurement was conducted using a live-cell imaging method with CellROX Deep Red reagent (Grinberg et al., 2013, 2012). Cells cultured in lrECM gel were smeared on slides. CellROX reagent at a final concentration of 5 µM in T4 medium or MCF-10A medium was added and the slides were incubated for 30 min at 37°C. Fluorescence images were acquired using an Eclipse 80i microscope (Nikon) with 532–587-nm excitation and 608–683-nm emission filters. The pictures were taken under fixed exposure conditions. Fluorescence intensity was quantitated using the NIS-Elements AR software (Nikon).

Immunofluorescence assay

Cells cultured in lrECM gel were smeared on slides, dried briefly, fixed with 4% paraformaldehyde and permeabilized with 0.5% Triton X-100. After blocking with 10% goat serum at room temperature for 60 min, specimens were incubated with primary antibody (anti-Integrin α6 antibody, 1:500 dilution; anti-Ki-67 antibody, 1:250 dilution) overnight at 4°C. Specimens were washed three times with immunofluorescence buffer (130 mM NaCl, 3.5 mM NaH_2PO_4, 7 mM Na_2HPO_4, pH 7.2, 7.7 mM NaN_3, 0.1% bovine serum albumin, 0.2% Triton X-100, 0.05% Tween-20) and incubated in fluorochrome-conjugated secondary antibody (1:500 dilution) for 1 h at room temperature in the dark. Stained samples were imaged with an Eclipse 80i microscope (Nikon) or an Olympus FV1000 confocal microscope.

Cell proliferation was assessed by quantification of proportion of cells with Ki-67-positive staining. The number of nuclei positive for Ki-67 antigen was counted and divided by the total number of nuclei, which were stained with DAPI.

qRT-PCR

Total RNA was extracted from cells using Trizol reagent (Invitrogen). cDNA was synthesized by using a SuperScript First Strand Synthesis kit (Invitrogen) from 1.0 µg RNA samples. qRT-PCR reactions were carried out using SYBR Green PCR master mix reagents (Thermo Scientific) on an ABI StepOnePlus Real-Time PCR System (Applied Biosystems). Thermal cycling was conducted at 95°C for 30 s, followed by 40 cycles of amplification at 95°C for 5 s, 55°C for 30 s and 72°C for 15 s. The relative quantification of gene expression for each sample was analyzed by the ΔCt method. The following primers were used to amplify: *IL-6*, 5′-ACTCAC-CTCTTCAGAACGAATTG-3′ and 5′-CCATCTTTGGAAGGTTCAGG-TTG-3′; *IL-8*, 5′-TTTTGCCAAGGAGTGCTAAAGA-3′ and 5′-AACC-CTCTGCACCCAGTTTTC-3′; *IL-24*, 5′-TGTGAAAGACACTATGCAA-GCTC-3′ and 5′-GTGACACGATGAGAACAAAGTTG-3′; *IL-32*, 5′-G-CTTCCCGAAGGTCCTCTCT-3′ and 5′-ATAAGCCGCCACTGTCTCC-A-3′; *CXCL1*, 5′-GCTCTTCCGCTCCTCTCACA-3′ and 5′-GGGGACT-TCACGTTCACACTT-3′; *CXCL2*, 5′-TCGCACAGCCGCTCGAA-3′ and 5′-GGGGACTTCACCTTCACACTTTG-3′; *CXCL3*, 5′-TGAATGTAAG-GTCCCCCGGA-3′ and 5′-CACCCTGCAGGAAGTGTCAA-3′; *CXCL6*, 5′-GACAGAGCTGCGTTGCACTT-3′ and 5′-CGGGTCCAGACAAA-CTTGCTT-3′; *18S* rRNA, 5′-ACCTGGTTGATCCTGCCAGT-3′ and 5′-CTGACCGGGTTGGTTTTGAT-3′.

Conditioned medium collection and ELISA assay

After HMT-3522 mammary epithelial cells were cultured in 3D lrECM gel for 3 days, culture medium was replaced with fresh T4 medium and incubated for an additional 48 h. Conditioned medium was collected, centrifuged at 4058 ***g*** for 5 min to pellet floating cells and debris. The supernatant was analyzed for secreted IL-6 (Biolegend, 430504) and CXCL1 (Abcam, ab100530) by ELISA assay according to the manufacturer's instructions.

Luciferase assay

T4-2 cells were co-transfected with NF-κB-luciferase (Addgene plasmid # 26699) and pNeo plasmid (1:10) according to previously described methods (Becker-Weimann et al., 2013; Mitchell and Sugden, 1995). Stably transfected clones were isolated by G418 selection and selected by luciferase reporter assay (50 µg/ml, 2 weeks), and then one positive clone was stably transfected with virus containing Rac1 L61 or Myr-Akt expression constructs. Following treatment, luciferase activity was measured using the Dual-Luciferase Reporter Assay System (Promega) and a Sirius luminometer (Berthold Detection Systems, Pforzheim, Germany).

Western blot analysis

Western blotting was performed as previously described (Xiong et al., 2012). Protein expression was visualized using a LI-COR Odyssey infra-red imaging system at a 700-nm wavelength, and quantitative densitometry was performed using Image Studio Lite software.

Statistical analysis

Inferential statistics were used to compare data sets from different experimental groups and reported data are the mean±s.e.m. Student's *t*-tests (two groups) and one-way ANOVA (three or more groups) were used to determine the significant differences between means, and were performed with SigmaPlot 12.3 (Systat Software Inc., San Jose, CA). The minimum statistical significance was set at $P<0.05$.

Acknowledgements

The authors are grateful to Mina J. Bissell for her support in this study and providing HMT-3522 cell lines. The authors thank the Research Communications Office at the Markey Cancer Center for assistance with manuscript preparation.

Competing interests

The authors declare no competing or financial interests.

Author contributions

R.X. and W.X. conceived the work, designed the experiments, supervised its analysis and edited the manuscript. L.L. designed the experiments and performed most of the experiments, collected and analyzed the data, and drafted the manuscript. D.K.S. conceived the work and revised the manuscript. J.C. and G.X. carried out some experiments.

Funding

This study was supported by start-up funding from the Markey Cancer Center and funding support from the American Heart Association (12SDG8600000 to R.X.), U.S. Department of Defense (W81XWH-15-1-0052 to R.X.). L.L. was supported by a joint PhD scholarship (201406170144) from the China Scholarship Council. The contents of this manuscript are solely the responsibility of the authors and do not necessarily represent the official views of the funding agencies.

Supplementary information

Supplementary information available online at
http://jcs.biologists.org/lookup/doi/10.1242/jcs.186031.supplemental

References

Allavena, P., Sica, A., Garlanda, C. and Mantovani, A. (2008). The Yin-Yang of tumor-associated macrophages in neoplastic progression and immune surveillance. *Immunol. Rev.* **222**, 155-161.

Auwerx, J. (1991). The human leukemia cell line, THP-1: a multifacetted model for the study of monocyte-macrophage differentiation. *Experientia* **47**, 22-31.
Babior, B. M. (2000). Phagocytes and oxidative stress. *Am. J. Med.* **109**, 33-44.
Baldwin, A. S., Jr. (1996). The NF-kappa B and I kappa B proteins: new discoveries and insights. *Annu. Rev. Immunol.* **14**, 649-683.
Becker-Weimann, S., Xiong, G., Furuta, S., Han, J., Kuhn, I., Akavia, U.-D., Pe'er, D., Bissell, M. J. and Xu, R. (2013). NFkB disrupts tissue polarity in 3D by preventing integration of microenvironmental signals. *Oncotarget* **4**, 2010-2020.
Beliveau, A., Mott, J. D., Lo, A., Chen, E. I., Koller, A. A., Yaswen, P., Muschler, J. and Bissell, M. J. (2010). Raf-induced MMP9 disrupts tissue architecture of human breast cells in three-dimensional culture and is necessary for tumor growth in vivo. *Genes Dev.* **24**, 2800-2811.
Bilder, D. (2004). Epithelial polarity and proliferation control: links from the Drosophila neoplastic tumor suppressors. *Genes Dev.* **18**, 1909-1925.
Bissell, M. J. and Bilder, D. (2003). Polarity determination in breast tissue: desmosomal adhesion, myoepithelial cells, and laminin 1. *Breast Cancer Res.* **5**, 117-119.
Bissell, M. J., Radisky, D. C., Rizki, A., Weaver, V. M. and Petersen, O. W. (2002). The organizing principle: microenvironmental influences in the normal and malignant breast. *Differentiation* **70**, 537-546.
Boghaert, E., Radisky, D. C. and Nelson, C. M. (2014). Lattice-based model of ductal carcinoma in situ suggests rules for breast cancer progression to an invasive state. *PLoS Comput. Biol.* **10**, e1003997.
Bubici, C., Papa, S., Dean, K. and Franzoso, G. (2006). Mutual cross-talk between reactive oxygen species and nuclear factor-kappa B: molecular basis and biological significance. *Oncogene* **25**, 6731-6748.
Bunker, B. D., Nellimoottil, T. T., Boileau, R. M., Classen, A. K. and Bilder, D. (2015). The transcriptional response to tumorigenic polarity loss in Drosophila. *Elife* **4**, e03189.
Cairns, R. A., Harris, I. S. and Mak, T. W. (2011). Regulation of cancer cell metabolism. *Nat. Rev. Cancer* **11**, 85-95.
Chance, B., Sies, H. and Boveris, A. (1979). Hydroperoxide metabolism in mammalian organs. *Physiol. Rev.* **59**, 527-605.
Cheng, G., Diebold, B. A., Hughes, Y. and Lambeth, J. D. (2006). Nox1-dependent reactive oxygen generation is regulated by Rac1. *J. Biol. Chem.* **281**, 17718-17726.
Chiarugi, P., Pani, G., Giannoni, E., Taddei, L., Colavitti, R., Raugei, G., Symons, M., Borrello, S., Galeotti, T. and Ramponi, G. (2003). Reactive oxygen species as essential mediators of cell adhesion: the oxidative inhibition of a FAK tyrosine phosphatase is required for cell adhesion. *J. Cell Biol.* **161**, 933-944.
Colotta, F., Allavena, P., Sica, A., Garlanda, C. and Mantovani, A. (2009). Cancer-related inflammation, the seventh hallmark of cancer: links to genetic instability. *Carcinogenesis* **30**, 1073-1081.
Cooke, M. S., Evans, M. D., Dizdaroglu, M. and Lunec, J. (2003). Oxidative DNA damage: mechanisms, mutation, and disease. *FASEB J.* **17**, 1195-1214.
Coussens, L. M. and Werb, Z. (2002). Inflammation and cancer. *Nature* **420**, 860-867.
Debnath, J. and Brugge, J. S. (2005). Modelling glandular epithelial cancers in three-dimensional cultures. *Nat. Rev. Cancer* **5**, 675-688.
Debnath, J., Muthuswamy, S. K. and Brugge, J. S. (2003). Morphogenesis and oncogenesis of MCF-10A mammary epithelial acini grown in three-dimensional basement membrane cultures. *Methods* **30**, 256-268.
DeNardo, D. G. and Coussens, L. M. (2007). Inflammation and breast cancer. Balancing immune response: crosstalk between adaptive and innate immune cells during breast cancer progression. *Breast Cancer Res.* **9**, 212.
DeNardo, D. G., Brennan, D. J., Rexhepaj, E., Ruffell, B., Shiao, S. L., Madden, S. F., Gallagher, W. M., Wadhwani, N., Keil, S. D., Junaid, S. A. et al. (2011). Leukocyte complexity predicts breast cancer survival and functionally regulates response to chemotherapy. *Cancer Discov.* **1**, 54-67.
Droge, W. (2002). Free radicals in the physiological control of cell function. *Physiol. Rev.* **82**, 47-95.
Dvorak, H. F. (1986). Tumors: wounds that do not heal. Similarities between tumor stroma generation and wound healing. *N. Engl. J. Med.* **315**, 1650-1659.
Ewald, A. J., Huebner, R. J., Palsdottir, H., Lee, J. K., Perez, M. J., Jorgens, D. M., Tauscher, A. N., Cheung, K. J., Werb, Z. and Auer, M. (2012). Mammary collective cell migration involves transient loss of epithelial features and individual cell migration within the epithelium. *J. Cell Sci.* **125**, 2638-2654.
Finkel, T. (2003). Oxidant signals and oxidative stress. *Curr. Opin. Cell Biol.* **15**, 247-254.
Finkel, T. (2011). Signal transduction by reactive oxygen species. *J. Cell Biol.* **194**, 7-15.
Gloire, G., Legrand-Poels, S. and Piette, J. (2006). NF-kappaB activation by reactive oxygen species: fifteen years later. *Biochem. Pharmacol.* **72**, 1493-1505.
Gouon-Evans, V., Rothenberg, M. E. and Pollard, J. W. (2000). Postnatal mammary gland development requires macrophages and eosinophils. *Development* **127**, 2269-2282.
Grinberg, Y. Y., van Drongelen, W. and Kraig, R. P. (2012). Insulin-like growth factor-1 lowers spreading depression susceptibility and reduces oxidative stress. *J. Neurochem.* **122**, 221-229.
Grinberg, Y. Y., Dibbern, M. E., Levasseur, V. A. and Kraig, R. P. (2013). Insulin-like growth factor-1 abrogates microglial oxidative stress and TNF-alpha responses to spreading depression. *J. Neurochem.* **126**, 662-672.
Gudjonsson, T., Ronnov-Jessen, L., Villadsen, R., Rank, F., Bissell, M. J. and Petersen, O. W. (2002). Normal and tumor-derived myoepithelial cells differ in their ability to interact with luminal breast epithelial cells for polarity and basement membrane deposition. *J. Cell Sci.* **115**, 39-50.
Hanahan, D. and Weinberg, R. A. (2011). Hallmarks of cancer: the next generation. *Cell* **144**, 646-674.
Hoesel, B. and Schmid, J. A. (2013). The complexity of NF-kappaB signaling in inflammation and cancer. *Mol. Cancer* **12**, 86.
Ingman, W. V., Wyckoff, J., Gouon-Evans, V., Condeelis, J. and Pollard, J. W. (2006). Macrophages promote collagen fibrillogenesis around terminal end buds of the developing mammary gland. *Dev. Dyn.* **235**, 3222-3229.
Inman, J. L. and Bissell, M. J. (2010). Apical polarity in three-dimensional culture systems: where to now? *J. Biol.* **9**, 2.
Kamp, D. W., Shacter, E. and Weitzman, S. A. (2011). Chronic inflammation and cancer: the role of the mitochondria. *Oncology* **25**, 400-410, 413.
Karin, M. (2006). Nuclear factor-kappaB in cancer development and progression. *Nature* **441**, 431-436.
Karin, M. (2009). NF-kappaB as a critical link between inflammation and cancer. *Cold Spring Harb. Perspect. Biol.* **1**, a000141.
Kenny, P. A., Lee, G. Y., Myers, C. A., Neve, R. M., Semeiks, J. R., Spellman, P. T., Lorenz, K., Lee, E. H., Barcellos-Hoff, M. H., Petersen, O. W. et al. (2007). The morphologies of breast cancer cell lines in three-dimensional assays correlate with their profiles of gene expression. *Mol. Oncol.* **1**, 84-96.
Kim, K.-J., Cho, K.-D., Jang, K. Y., Kim, H.-A., Kim, H.-K., Lee, H.-K. and Im, S.-Y. (2014). Platelet-activating factor enhances tumour metastasis via the reactive oxygen species-dependent protein kinase casein kinase 2-mediated nuclear factor-kappaB activation. *Immunology* **143**, 21-32.
Kroncke, K.-D. (2003). Nitrosative stress and transcription. *Biol. Chem.* **384**, 1365-1377.
Kumar, S. and Sitasawad, S. L. (2009). N-acetylcysteine prevents glucose/glucose oxidase-induced oxidative stress, mitochondrial damage and apoptosis in H9c2 cells. *Life Sci.* **84**, 328-336.
Lee, M. and Vasioukhin, V. (2008). Cell polarity and cancer–cell and tissue polarity as a non-canonical tumor suppressor. *J. Cell Sci.* **121**, 1141-1150.
Leek, R. D., Lewis, C. E., Whitehouse, R., Greenall, M., Clarke, J. and Harris, A. L. (1996). Association of macrophage infiltration with angiogenesis and prognosis in invasive breast carcinoma. *Cancer Res.* **56**, 4625-4629.
Lelievre, S. A., Weaver, V. M., Nickerson, J. A., Larabell, C. A., Bhaumik, A., Petersen, O. W. and Bissell, M. J. (1998). Tissue phenotype depends on reciprocal interactions between the extracellular matrix and the structural organization of the nucleus. *Proc. Natl. Acad. Sci. USA* **95**, 14711-14716.
Li, N. and Karin, M. (1999). Is NF-kappaB the sensor of oxidative stress? *FASEB J.* **13**, 1137-1143.
Liu, H., Radisky, D. C., Wang, F. and Bissell, M. J. (2004). Polarity and proliferation are controlled by distinct signaling pathways downstream of PI3-kinase in breast epithelial tumor cells. *J. Cell Biol.* **164**, 603-612.
Mahmoud, S. M. A., Lee, A. H. S., Paish, E. C., Macmillan, R. D., Ellis, I. O. and Green, A. R. (2012). Tumour-infiltrating macrophages and clinical outcome in breast cancer. *J. Clin. Pathol.* **65**, 159-163.
Martin-Belmonte, F. and Perez-Moreno, M. (2012). Epithelial cell polarity, stem cells and cancer. *Nat. Rev. Cancer* **12**, 23-38.
Medrek, C., Ponten, F., Jirstrom, K. and Leandersson, K. (2012). The presence of tumor associated macrophages in tumor stroma as a prognostic marker for breast cancer patients. *BMC Cancer* **12**, 306.
Miao, L. and St Clair, D. K. (2009). Regulation of superoxide dismutase genes: implications in disease. *Free Radic. Biol. Med.* **47**, 344-356.
Mitchell, T. and Sugden, B. (1995). Stimulation of NF-kappa B-mediated transcription by mutant derivatives of the latent membrane protein of Epstein-Barr virus. *J. Virol.* **69**, 2968-2976.
Moller, P. and Wallin, H. (1998). Adduct formation, mutagenesis and nucleotide excision repair of DNA damage produced by reactive oxygen species and lipid peroxidation product. *Mutat. Res.* **410**, 271-290.
Morgan, M. J. and Liu, Z.-G. (2011). Crosstalk of reactive oxygen species and NF-kappaB signaling. *Cell Res.* **21**, 103-115.
Murdoch, C., Giannoudis, A. and Lewis, C. E. (2004). Mechanisms regulating the recruitment of macrophages into hypoxic areas of tumors and other ischemic tissues. *Blood* **104**, 2224-2234.
Muthuswamy, S. K. and Xue, B. (2012). Cell polarity as a regulator of cancer cell behavior plasticity. *Annu. Rev. Cell Dev. Biol.* **28**, 599-625.
Nathan, C. (2002). Points of control in inflammation. *Nature* **420**, 846-852.
Nelson, C. M. and Bissell, M. J. (2006). Of extracellular matrix, scaffolds, and signaling: tissue architecture regulates development, homeostasis, and cancer. *Annu. Rev. Cell Dev. Biol.* **22**, 287-309.
Petersen, O. W., Ronnov-Jessen, L., Howlett, A. R. and Bissell, M. J. (1992). Interaction with basement membrane serves to rapidly distinguish growth and differentiation pattern of normal and malignant human breast epithelial cells. *Proc. Natl. Acad. Sci. USA* **89**, 9064-9068.

Puri, P. L., Bhakta, K., Wood, L. D., Costanzo, A., Zhu, J. and Wang, J. Y. J. (2002). A myogenic differentiation checkpoint activated by genotoxic stress. *Nat. Genet.* **32**, 585-593.

Radisky, D. C., Levy, D. D., Littlepage, L. E., Liu, H., Nelson, C. M., Fata, J. E., Leake, D., Godden, E. L., Albertson, D. G., Nieto, M. A. et al. (2005). Rac1b and reactive oxygen species mediate MMP-3-induced EMT and genomic instability. *Nature* **436**, 123-127.

Rejon, C. and McCaffrey, L. (2015). Cell polarity in mammary gland morphogenesis and breast cancer. In *Cell Polarity 2: Role in Development and Disease* (ed. K. Ebnet), pp. 187-207. Switzerland: Springer International Publishing.

Reuter, S., Gupta, S. C., Chaturvedi, M. M. and Aggarwal, B. B. (2010). Oxidative stress, inflammation, and cancer: how are they linked? *Free Radic. Biol. Med.* **49**, 1603-1616.

Schreck, R., Rieber, P. and Baeuerle, P. A. (1991). Reactive oxygen intermediates as apparently widely used messengers in the activation of the NF-kappa B transcription factor and HIV-1. *EMBO J.* **10**, 2247-2258.

Sharma, M., Beck, A. H., Webster, J. A., Espinosa, I., Montgomery, K., Varma, S., van de Rijn, M., Jensen, K. C. and West, R. B. (2010). Analysis of stromal signatures in the tumor microenvironment of ductal carcinoma in situ. *Breast Cancer Res. Treat.* **123**, 397-404.

St Johnston, D. and Ahringer, J. (2010). Cell polarity in eggs and epithelia: parallels and diversity. *Cell* **141**, 757-774.

Tepass, U. (2012). The apical polarity protein network in Drosophila epithelial cells: regulation of polarity, junctions, morphogenesis, cell growth, and survival. *Annu. Rev. Cell Dev. Biol.* **28**, 655-685.

Tsuchiya, S., Yamabe, M., Yamaguchi, Y., Kobayashi, Y., Konno, T. and Tada, K. (1980). Establishment and characterization of a human acute monocytic leukemia cell line (THP-1). *Int. J. Cancer* **26**, 171-176.

Tsuchiya, S., Kobayashi, Y., Goto, Y., Okumura, H., Nakae, S., Konno, T. and Tada, K. (1982). Induction of maturation in cultured human monocytic leukemia cells by a phorbol diester. *Cancer Res.* **42**, 1530-1536.

Valko, M., Rhodes, C. J., Moncol, J., Izakovic, M. and Mazur, M. (2006). Free radicals, metals and antioxidants in oxidative stress-induced cancer. *Chem. Biol. Interact.* **160**, 1-40.

Vepa, S., Scribner, W. M., Parinandi, N. L., English, D., Garcia, J. G. and Natarajan, V. (1999). Hydrogen peroxide stimulates tyrosine phosphorylation of focal adhesion kinase in vascular endothelial cells. *Am. J. Physiol.* **277**, L150-L158.

Wang, H. H., Ducatman, B. S. and Eick, D. (1989). Comparative features of ductal carcinoma in situ and infiltrating ductal carcinoma of the breast on fine-needle aspiration biopsy. *Am. J. Clin. Pathol.* **92**, 736-740.

Wang, X., Gu, C., He, W., Ye, X., Chen, H., Zhang, X. and Hai, C. (2012). Glucose oxidase induces insulin resistance via influencing multiple targets in vitro and in vivo: the central role of oxidative stress. *Biochimie* **94**, 1705-1717.

Waris, G. and Ahsan, H. (2006). Reactive oxygen species: role in the development of cancer and various chronic conditions. *J. Carcinog.* **5**, 14.

Weaver, V. M., Petersen, O. W., Wang, F., Larabell, C. A., Briand, P., Damsky, C. and Bissell, M. J. (1997). Reversion of the malignant phenotype of human breast cells in three-dimensional culture and in vivo by integrin blocking antibodies. *J. Cell Biol.* **137**, 231-245.

Weaver, V. M., Lelievre, S., Lakins, J. N., Chrenek, M. A., Jones, J. C. R., Giancotti, F., Werb, Z. and Bissell, M. J. (2002). beta4 integrin-dependent formation of polarized three-dimensional architecture confers resistance to apoptosis in normal and malignant mammary epithelium. *Cancer Cell* **2**, 205-216.

Wiseman, H. and Halliwell, B. (1996). Damage to DNA by reactive oxygen and nitrogen species: role in inflammatory disease and progression to cancer. *Biochem. J.* **313**, 17-29.

Xiong, G., Wang, C., Evers, B. M., Zhou, B. P. and Xu, R. (2012). RORalpha suppresses breast tumor invasion by inducing SEMA3F expression. *Cancer Res.* **72**, 1728-1739.

Xu, R., Nelson, C. M., Muschler, J. L., Veiseh, M., Vonderhaar, B. K. and Bissell, M. J. (2009). Sustained activation of STAT5 is essential for chromatin remodeling and maintenance of mammary-specific function. *J. Cell Biol.* **184**, 57-66.

Xu, R., Spencer, V. A., Groesser, D. L. and Bissell, M. J. (2010). Laminin regulates PI3K basal localization and activation to sustain STAT5 activation. *Cell Cycle* **9**, 4315-4322.

Zeitler, J., Hsu, C. P., Dionne, H. and Bilder, D. (2004). Domains controlling cell polarity and proliferation in the Drosophila tumor suppressor Scribble. *J. Cell Biol.* **167**, 1137-1146.

Zhang, Y., Cheng, S., Zhang, M., Zhen, L., Pang, D., Zhang, Q. and Li, Z. (2013). High-infiltration of tumor-associated macrophages predicts unfavorable clinical outcome for node-negative breast cancer. *PLoS ONE* **8**, e76147.

Zhao, Y. and Davis, H. W. (1998). Hydrogen peroxide-induced cytoskeletal rearrangement in cultured pulmonary endothelial cells. *J. Cell Physiol.* **174**, 370-379.